Physics of Fluids

The precise and accurate production of millimetric water droplets using a superhydrophobic generating apparatus

Cite as: Phys. Fluids **30**, 027104 (2018); https://doi.org/10.1063/1.5009929
Submitted: 20 October 2017 • Accepted: 27 January 2018 • Published Online: 15 February 2018

Michael J. Wood, Felipe Aristizabal, Matthew Coady, et al.

The precise and accurate production of millimetric water droplets using a superhydrophobic generating apparatus

Michael J. Wood,[1] Felipe Aristizabal,[1] Matthew Coady,[2] Kent Nielson,[3] Paul J. Ragogna,[2] and Anne-Marie Kietzig[1,a)]

[1]*Department of Chemical Engineering, McGill University, Montréal, Quebec H3A 0C5, Canada*
[2]*Department of Chemistry, University of Western Ontario, London, Ontario N6A 3K7, Canada*
[3]*Product Innovation Lab, 3M Canada Company, London, Ontario N5V 3R6, Canada*

(Received 20 October 2017; accepted 27 January 2018; published online 15 February 2018)

The production of millimetric liquid droplets has importance in a wide range of applications both in the laboratory and industrially. As such, much effort has been put forth to devise methods to generate these droplets on command in a manner which results in high diameter accuracy and precision, well-defined trajectories followed by successive droplets and low oscillations in droplet shape throughout their descents. None of the currently employed methods of millimetric droplet generation described in the literature adequately addresses all of these desired droplet characteristics. The reported methods invariably involve the cohesive separation of the desired volume of liquid from the bulk supply in the same step that separates the single droplet from the solid generator. We have devised a droplet generation device which separates the desired volume of liquid within a tee-apparatus in a step prior to the generation of the droplet which has yielded both high accuracy and precision of the diameters of the final droplets produced. Further, we have engineered a generating tip with extreme antiwetting properties which has resulted in reduced adhesion forces between the liquid droplet and the solid tip. This has yielded the ability to produce droplets of low mass without necessitating different diameter generating tips or the addition of surfactants to the liquid, well-defined droplet trajectories, and low oscillations in droplet volume. The trajectories and oscillations of the droplets produced have been assessed and presented quantitatively in a manner that has been lacking in the current literature. *Published by AIP Publishing.* https://doi.org/10.1063/1.5009929

I. INTRODUCTION

The production and manipulation of liquid droplets whose diameters are in the millimetric range is of importance to a wide range of industrial applications and laboratory investigations. An inexhaustive list includes the filling of each individual pixel with liquid crystals for the production of digital displays,[1] the precise placement of liquid adhesives in intricate applications,[2] the printing of photoresist masks for the manufacturing of circuit boards,[3] the encapsulation of biological components for enhanced control and sustained therapeutic effect,[4–6] and any scientific research involving the study of droplet interaction.[7]

In any of the aforementioned industrial and laboratory examples, the droplet generation/manipulation steps are judged upon their ability to repeatedly produce a (single) droplet on demand of a prescribed volume. Of equal importance to this step's efficacy is the manner in which the droplet behaves after production. A droplet that has little oscillation in volume upon detachment from the generating device is surely desired such that any later interaction of said droplet with a surface or other liquid is also reproducible.[8–11] In the same line of thinking, it is also desirable to have all of the liquid droplets follow the same path from the generating device to the target such that the droplets land in the exact same location after every instance of production. Despite the importance of these droplet characteristics, neither droplet oscillation nor droplet trajectory is quantified in the current literature which discusses methods of generation.[12–20]

The production of droplets invariably involves the contact between the solid surface of the generating tip and a portion of the surface area of the liquid droplet. A balance of the forces acting on a pendant droplet hanging at the end of a capillary is shown graphically in Fig. 1. The hanging droplet is subjected to the adhesive force due to surface tension, σ, which acts through the boundary length of the circumference of the generating tip. The upward adhesive force is balanced with the vertical gravitational force, mg, according to Eq. (1).[21] The limit of Eq. (1) is reached when θ approaches 90° and leads directly to Tate's law, Eq. (2). Thus, the diameter of the droplet which will detach under its own weight from a hanging pendant is linked inextricably to the boundary length between the liquid and the generating tip and the surface tension of the generated liquid,[22]

$$mg = 2\pi r\sigma \sin\theta, \tag{1}$$

$$mg = 2\pi r\sigma. \tag{2}$$

Many of the methods currently employed in the laboratory (or industrially) to produce liquid droplets in the millimetric diameter range focus on the manipulation of the force balance on the **hanging pendant** to achieve droplets within the

a)Author to whom correspondence should be addressed: anne.kietzig@mcgill.ca

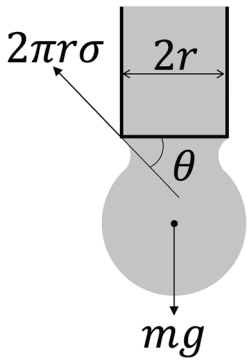

FIG. 1. A force balance on a liquid pendant hanging from a droplet generating tip.

range of the desired diameter. The most common technique used is to dispense the liquid through a stainless steel dispensing tip of appropriate diameter.[23–26] However, the smallest droplet that is produceable with this method, using the smallest commercially available dispensing tip, is 1.8 mm. Reil and Hallett overcame the limitations in droplet diameter accuracy and precision associated with the hanging pendant method by building a device with an intermittent air flow concentric to the syringe tip.[12] More recently, Mao *et al.* induced oscillations in pendants hanging on the end of a capillary.[13] These **forced pendant** methods result in hanging pendants with masses smaller than the critical mass for gravitational detachment prescribed by Tate's law being dislodged by the application of the additional downward force of the burst of compressed gas or oscillations.

Other methods of droplet generation forgo detaching a hanging pendant. Instead, some methods apply pressure waves on liquid in a nozzle through a short burst of pressurized gas, in the case of the **pneumatic pressure wave** method, or the flexion of a piezoelectric element, in the case of the **piezoelectric pressure wave** method. These two pressure wave techniques are often broadly referred to as *drop-on-demand*. In this manner, the liquid surface at the tip of the nozzle is oscillated to the point that the formed jet becomes extended so much that it will no longer fully retract due to the liquid's surface tension. The extended jet begins to neck, with eventual total separation of a volume of liquid from the bulk supply.[14,15,27] This volume of liquid that is left behind from the retreating liquid front forms the generated droplet and begins to descend from the generator. The drop-on-demand mode of generating droplets is often touted for its ease of use and high speed of generation.[16] However, as summarized in a review by Derby, these systems all operate within a narrow regime of Weber ($We = v^2\rho d/\sigma$) and Reynolds ($Re = v\rho d/\mu$) numbers.[17] Where ρ, μ, and d are the droplet density, dynamic viscosity, and diameter, respectively. Duineveld *et al.* determined that droplets require a minimum velocity, $v_{\min}$, (and hence minimum *We*) to be ejected from the generating tip, as given by Eq. (3).[28] Further, the ratio between the droplet's viscosity, inertial forces, and surface tension forces must reside in the range given by Eq. (4).[29] Low *Re* liquids (such as those with high viscosity) tend to dampen the pressure waves,

TABLE I. Positive and negative characteristics of the currently employed millimetric droplet generation methods.

Droplet generation method	Positive characteristics	Negative characteristics
Hanging pendant[22–26]	Narrow range in the spread of droplet diameters	Generation of one droplet size per dispensing tip/liquid combination
Forced pendant[12,13]	Narrow range in the spread of droplet diameters	Considerable droplet oscillations during descent due to burst gas-induced perturbations
	Production of droplets with masses less than the critical mass for gravitational detachment	Droplets tend to not follow a prescribed trajectory.
Pneumatic pressure wave[15,20]	Production of droplets with diameters smaller than the pendant methods High ease of use	Generation of one droplet size per dispensing tip/liquid combination Production of abnormally large or small droplets not uncommon Cohesive breakup of the liquid jet results in stochastic production of satellite droplets and high degree of oscillation Droplets tend to not follow a prescribed trajectory
Piezoelectric pressure wave[14,16,18,20]	Production of droplets with diameters down to the diameter of the dispensing tip	Requires optimization of frequency/amplitude of piezoelectric element flexion for each small range of droplet diameters and liquid desired
	High ease of use and high speed of droplet generation	Cohesive breakup of the liquid jet results in stochastic production of satellite droplets and high degree of oscillation Droplets tend to not follow a prescribed trajectory
Rayleigh stream breakup[19,30,31]	Production of droplets with high diameter precision High speed of droplet generation	Produces a stream of droplets; no single droplet production capability

preventing droplet ejection. High *Re* liquids, however, result in the production of a large number of satellite droplets,[18,19]

$$We = v_{\min}\sqrt{\frac{\rho d_{nozzle}}{\sigma}} > 4, \tag{3}$$

$$1 < \frac{Re}{\sqrt{We}} = \frac{\sqrt{\sigma \rho d_{nozzle}}}{\mu} < 10. \tag{4}$$

The breakup of a liquid stream into individual droplets by acoustic waves, so-called **Rayleigh stream breakup**, is often presented as an alternative to the drop-on-demand techniques. However, the Rayleigh breakup produces a constant stream of droplets. Many applications, however, necessitate a single droplet whose production can be accurately timed.[19,30,31]

The positive and negative attributes of the currently employed droplet generation techniques are summarized in Table I. The problems inherent to the existing methods of droplet generation can be attributed to two factors: (1) separating a desired volume of liquid from the bulk supply and (2) detachment of the liquid from the solid generating tip.

Here we present a droplet generating method that circumvents these two problematic factors with two separate solutions. (1) It was hypothesized that separating the desired quantity of liquid in a step prior to generating it into a droplet would offer a solution to the volume accuracy and precision problems. Rather than selecting the droplet volume in a stochastic cohesive breakup event, we propose the use of a tee-apparatus which would serve to facilitate the separation of a desired quantity of liquid from a bulk supply in a more gentle, predictable, and repeatable fashion. (2) It was hypothesized that the trajectory and volume oscillation issues could be solved by manipulating the force balance on the droplet through engineering of the solid surface rather than the application of additional forces or the addition of surfactants to the liquid. A minimized liquid-solid interaction by creation of a heterogeneous wetting state would, in theory, result in the droplet falling vertically downward with minimal oscillations in its volume throughout the descent. Further, we present herein a quantitative assessment of the volume oscillations and trajectories of the generated droplets that has been lacking from the current literature.

II. EXPERIMENTAL SETUP AND PROCEDURE

A. Fabrication and design of tee-apparatus

A tee-apparatus was constructed into a 25 × 25 × 5 mm block of polycarbonate by drilling two perpendicular channels, as is shown in Fig. 2(a). The holes were drilled such that their diameters equaled that of the outer diameter of 0.64 mm syringe tips. Syringe tips were mounted in hole number 1 and hole number 2 to introduce air and liquid, respectively. Upon removal of its *Luer-lok*, another syringe tip is fit into hole number 3 which serves as the outlet of the tee-apparatus as well as the mounting point for a superhydrophobic polytetrafluoroethylene tip. The syringe tips are held in place by *Loctite* 3103 UV-cured adhesive (Henkel Corporation).

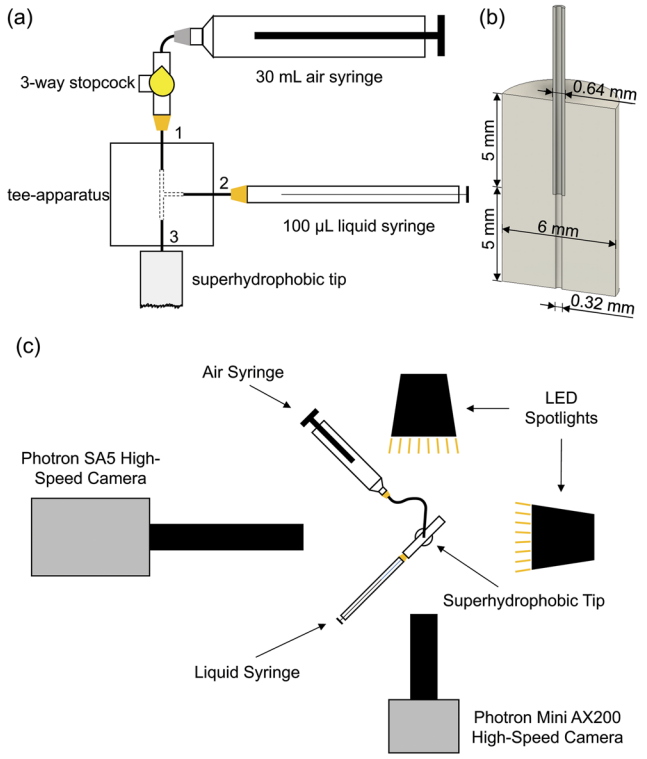

FIG. 2. (a) Schematic representation of the assembled superhydrophobic droplet generator. (b) Cross-sectional view of the PTFE generating tip. (c) Overhead view of the droplet measurement setup.

B. Fabrication and design of the superhydrophobic tip

Polytetrafluoroethylene (PTFE) was chosen as a base material for the droplet generating tip because of its machinability and its high intrinsic water contact angle.[32] A PTFE cylinder (McMaster-Carr) of 10 mm length and 6 mm diameter was machined with a 5 mm long 0.64 mm diameter hole through its axis from one end (matching the outer diameter of the tee-apparatus syringe tips) and a 0.32 mm diameter hole from the other end (matching the inner diameter of the syringe tips) as shown in Fig. 2(b). The inner dimension of the syringe tip selected ensures that during droplet production liquid is forced through a channel of constant diameter. This forces the liquid to travel through the tee as a cohesive plug. The end of the drilled PTFE cylinder was polished with 1200-grit polishing disks and then sonicated in acetone in preparation for femtosecond laser micromachining.

A *Coherent Libra* Ti:sapphire femtosecond laser system (Coherent, Inc.) was used to impart the laser-induced surface structures onto the PTFE, rendering it superhydrophobic.[32] This system has a wavelength of 800 nm, pulse duration <250 fs, repetition rate of 1 kHz, and a maximal output power of 4 W. The laser beam power was reduced and controlled with a computer controlled attenuator comprised of a motorized half wave-plate and a polarizing beam splitter. The attenuated beam was then focused onto an *xyz*-translation stage (Newport Corporation) with a 100 mm converging lens. The stage movements and shutter (Uniblitz) openings were controlled by GOL3D software (GB&S). The methods of Liang *et al.* were followed to ablate a 3 mm × 3 mm patch over the bottom of

the cylinder such that the previously drilled hole lay within the ablated area.[32]

C. Scanning electron microscopy (SEM) of the laser micromachined surface

The laser-induced surface modifications were imaged using an *FEI Inspect F*50 scanning electron microscope (ThermoFisher Scientific, Inc.). All images were captured using a spot size of 2.0 and a voltage of 10.0 kV. In preparation for SEM, the PTFE tip was sonicated in acetone after ablation to remove any non-sintered nanoparticles from the surface. The polymeric substrate was then sputter coated with 10 nm of gold to render it conductive (SPI Supplies, Inc.).

Figure 3(a) shows that the femtosecond laser micromachining routine has resulted in the ablated patch surrounding the end of the hole drilled through the PTFE droplet generating tip. The highly fibrous structure seen in Figs. 3(b) and 3(c) promotes robust superhydrophobicity, the so-called Cassie wetting state, whereas a water droplet will be in contact with a small area of solid while trapping air within the high fraction of void space in the microstructure.[33] As explained by Liang *et al.*, no water contact angle values could be measured for the ablated patch, as a sessile drop could not be placed onto the superhydrophobic surface created.[32] This phenomenon occurred over the entire area of the patch, including where the drilled hole is situated, suggesting that the rim of the hole was sufficiently textured to promote superhydrophobicity as well.

D. Generation of water droplets

As is shown schematically in Fig. 2(a), the laser-machined PTFE tip is mounted to the end of the tee-apparatus to form the droplet generator. A set of syringe pumps were 3D printed using a design based on the one described by Wijnen *et al.* that was modified for the syringes in this application.[34] The syringe pumps were built using stepper motors (Trinamic Motion Control, Incorporated) with 200 steps/rotation and a linear actuating rod with M5 thread pitch of 0.8 mm. A 100 μl gas chromatography glass syringe with a 1.43 mm inside diameter barrel (Hamilton Company) supplied the reverse osmosis water into the tee through hole number 2. A 30 ml syringe (Cole-Parmer Company) supplied air through hole number 1. A three-way stopcock was installed between the air-supply syringe and the tee-apparatus to serve as a vent to the tee.

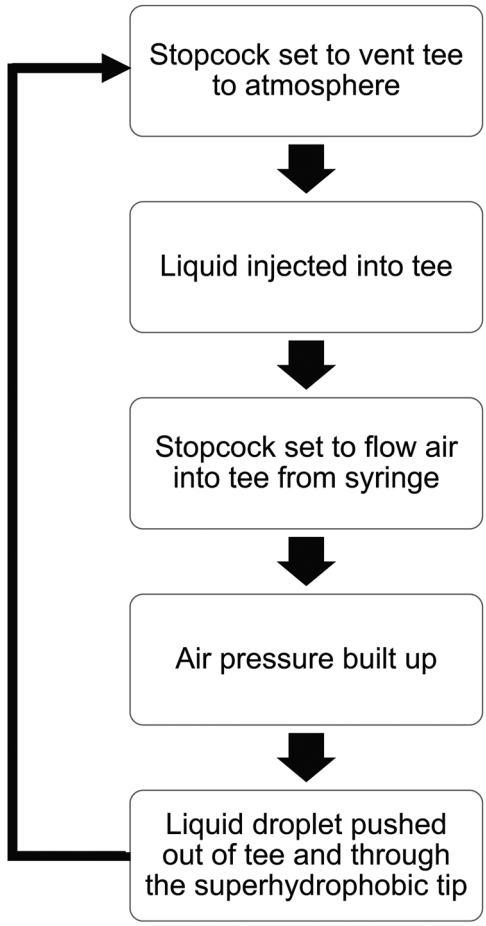

FIG. 4. Superhydrophobic droplet generation scheme flowchart.

The entire droplet generation scheme is shown in the flowchart of Fig. 4. The liquid stepper motor is activated for a prescribed number of steps, injecting water into the tee at a rate of 1200 nl/s. The plug of liquid formed in the tee is then pushed vertically down through the channel and out the superhydrophobic end by the pressure built up by the injection of air at a rate of 0.2 ml/s by the air syringe pump. Droplet production is automated through the use of an *Arduino Mega* 2560 microcontroller prototyping board (Arduino Company) equipped with a stepper motor shield (Adafruit, Incorporated). The stopcock is set automatically using a servo motor (Tower Pro, Incorporated) to allow the tee-apparatus to vent to the atmosphere. A video of the entire droplet production process using the superhydrophobic droplet generating apparatus is included in the supplementary material.

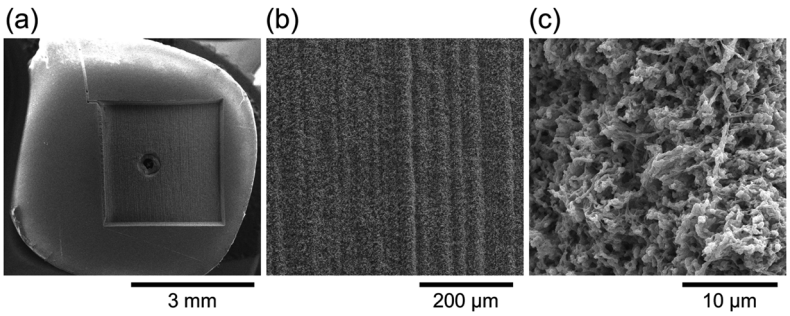

FIG. 3. Scanning electron micrographs of the femtosecond laser ablated PTFE droplet generating tip; (a) overview of the entire patch with the drilled hole in the middle; (b) the 89%-line overlap has imparted high surface homogeneity; (c) the microstructure is highly fibrous, leading to the Cassie wetting state.

E. Droplet measurements

Falling droplets were filmed with a pair of high-speed cameras, filming at 5000 frames/s and a shutter speed of 1/50 000 s (Photron *FastCam SA*5, *Mini AX*200). The high-speed cameras were set perpendicular to one another, with the superhydrophobic droplet generating device mounted at the nexus of their field of view, as shown in Fig. 2(c). The SA5 high-speed camera was equipped with a 6.5:1 telescope lens system with an infinity-corrected zoom module (Optem, Inc.), giving a resolution of 6.3 μm/pixel. The Mini AX200 was equipped with an 18-108 mm macro zoom lens (Navitar, Inc.), giving a resolution of 9.6 μm/pixel. High backlighting was provided by ultra-bright led spotlights (Optikon Corp.). The camera lenses were sufficiently zoomed in to provide filming of approximately 4 mm of falling height, balancing the need for fine measurements with the ability to record enough data points for analysis. In this configuration, the cameras remained stationary while the droplet generator was raised vertically using a translation stage to film the falling droplets at different heights during their descent.

Thirty droplets of each diameter tested were generated and filmed for each of the vertical positions of the droplet generator ($z = 0$, 5, 10, 15, 20, and 100 mm above the frame of filming). In total, 1370 high speed videos were captured and analyzed. Each frame of the captured videos, synchronized in time using Photron's software, contains a 2-dimensional projection of the falling droplet in two perpendicular planes. Thus, this two-camera experimental configuration yields an accurate measurement of droplet trajectory in 3-dimensions as well as a statistical tool to reduce variance in droplet diameters by measuring the physical object twice.

Image analysis techniques were applied to each individual frame of each camera's high-speed videos to perform the droplet measurements. The algorithm consists of three steps: (1) background subtraction, (2) thresholding, and (3) shape properties. Background subtraction distinguishes the falling droplet from the static components such as the PTFE tip or artifacts introduced by lighting conditions or camera lenses (e.g., dust particle). Selection of the threshold between descending droplet and video background was determined according to the methods of Otsu.[35] A set of statistical droplet shape properties were calculated from the analyzed videos according to Fig. 5. Each analyzed frame yields the droplet centroid ($\langle x', z' \rangle$) as well as major (D_{major}) and minor (D_{minor}) axes of an equivalent ellipse. Note that the droplet diameter measurement statistics presented herein quote a 95% prediction interval rather than a confidence interval on the mean.

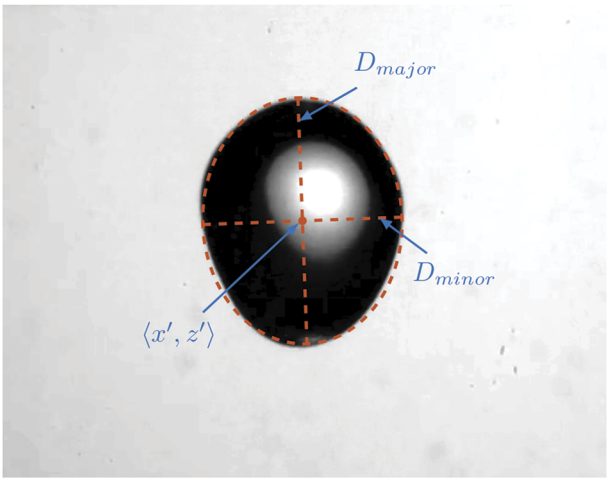

FIG. 5. Example of droplet measurements performed using image analysis: centroid ($\langle x', z' \rangle$) and major (D_{major}) and minor (D_{minor}) axes of equivalent ellipse.

III. RESULTS AND DISCUSSION

A. Water droplet size distribution

The first goal of the present work is to produce, on command, precise and accurately sized water droplets. Thus, the number of steps moved by the liquid-syringe pump stepper motor needs to correlate well with the diameter of the final droplet produced. Droplets were produced by injecting liquid through 700, 430, and 116 steps of the liquid syringe pump stepper motor into the tee-apparatus. The resulting average diameters measured for these experimental sets are presented in Fig. 6(a). The droplets produced using 700 steps have a diameter of 2.08 ± 0.11 mm. 430 steps of the liquid syringe pump have resulted in droplets with diameters of 1.79 ± 0.08 mm, while 116 steps have produced droplets with diameters of 1.10 ± 0.13 mm.

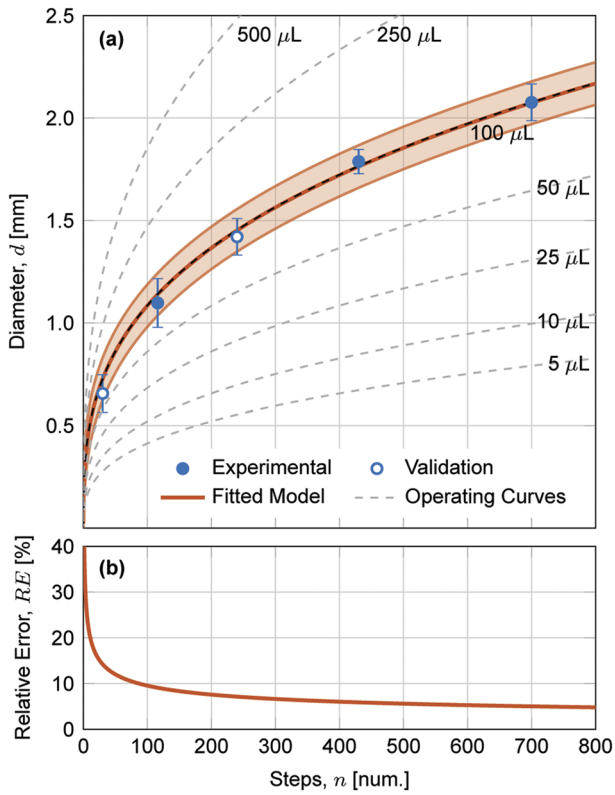

FIG. 6. (a) The average diameter and prediction intervals of water droplets produced using the novel superhydrophobic generating apparatus. The theoretical operating curve is both statistically fit to the experimental data and plotted using the physically derived fitting parameter, C. The statistics of two additional validation data sets are superposed and show high agreement with the model. (b) The relative error in the diameter of droplets produced per step of the liquid syringe pump presented as a function of the number of steps.

The number of steps moved by the liquid syringe pump stepper motor is theoretically directly related to the volume of droplet produced and related through a cubic relationship to the diameter of the droplet, as per Eq. (5), where n and D are the number of steps of the liquid syringe pump stepper motor and the diameter (in mm) of the droplet produced, respectively. C (having units of nl/step) is the proportionality parameter relating the number of steps taken by the stepper motor to the volume of liquid pushed out of the syringe, by the moving plunger, into the tee-apparatus,

$$D_{droplet} = \sqrt[3]{\frac{6}{\pi} C n_{steps}}. \tag{5}$$

The model presented in Eq. (5) was fit to the three data points to determine the single experimental fitting parameter, C_{exp}. The curve, fit using a least squares method, is presented as the dark line in Fig. 6(a), while the shaded area around the curve describes its 95% prediction interval. The value solved for C_{exp} is 6.68 ± 0.10 nl/step. Next we compared these experimental values to the physically derived fitting parameter. The degree of shaft rotation, θ_{motor}, to step ratio of the syringe pump stepper motor, the thread pitch of the linear actuating rod, $X_{actuator}/\theta_{actuator}$, and the volume of liquid dispensed, $V_{dispensed}$, in relation to the linear movement of the syringe plunger, $X_{plunger}$, all combine in Eq. (6) to allow for the calculation of the physical C-parameter, C_{phys}. C_{phys} of the liquid syringe pump built for these experiments was calculated to be 6.69 nl/step. The syringe pump operating curve of Eq. (5) is plotted in Fig. 6(a) using the physical C-parameter for this system. The 100 μl syringe operating curve is nearly indistinguishable from the model fit using C_{exp}, suggesting that the theory of operation presented herein is well understood and matches how the droplet generating apparatus performs in reality. This lends credence to the hypothesis presented that separating the desired quantity of liquid within the tee-apparatus in a step prior to the generation of the droplet offers great control over droplet volumes. Further, the tee-apparatus has proven itself to have no dead volume for the range of droplet diameters tested,

$$C_{phys} = \left(\frac{\theta_{motor}}{n_{motor}}\right)\left(\frac{X_{actuator}}{\theta_{actuator}}\right)\left(\frac{V_{dispensed}}{X_{plunger}}\right). \tag{6}$$

In addition, two data sets were collected as validation of the droplet generator's accuracy: one using 30 steps of the liquid syringe pump and another using 240 steps. The prediction intervals of both of these validation experiments are presented as overlays in Fig. 6(a). The validation data sets agree very well with the curve fit to the three full sets (and the operating curve derived using the physical parameters of the syringe pump), suggesting a high accuracy within the system presented here.

The spread in the diameters of the individual droplets measured shows that the system, as built, is highly precise. For context, the data presented here can be compared to the droplet diameters reported in published drop impact studies.[7,10,11] In those experiments, the diameter of the droplet impacting a solid surface is of utmost importance to the conclusions made. Aboud and Kietzig reported the use of droplet diameters of 0.95 ± 0.04 mm, which is a 4.2% error in diameter; Faβmann *et al.* presented their results having used droplets with a spread in diameters of 7%; and Stevens presented impact data collected using droplets whose diameters varied by 6.3%.[7,10,11] The measurements of these droplet diameter sets are presented as two *standard deviations*. Thus, the diameter of the droplets produced using the superhydrophobic droplet generator described herein exceeds the level of precision of those used in peer-reviewed articles for the 700 and 430 step data sets (having *prediction intervals* of 5.3% and 4.5% of the droplet diameters, respectively).

The prediction interval in measured droplet diameters increases markedly to 11.8% of the droplet diameter for the 116 step dataset. The cubic relationship between the number of steps taken by the liquid syringe pump and the diameter of the droplet produced means that for a given setup such as the one studied in the present work, small droplets require very few steps compared to larger droplets. Hence, the ratio between each millimetre of droplet diameter and each individual step is much larger for the small diameter droplets than for the large diameter droplets; this phenomenon is presented in Fig. 6(b). This ratio (and therefore the error in producing smaller diameter droplets) could be reduced by manipulating the C parameter through altering the physical setup of the liquid syringe pump. For the presently studied droplet generator, it was shown that C = 6.69 nl/step. This parameter could be reduced by swapping syringes for one with a smaller barrel, changing the thread pitch on the linear actuating rod, or adding gears between the motor and the linear actuator. Changes to the cubic relationship between the number of steps taken by the liquid syringe pump and the diameter of the droplet produced for varying volumes of *Hamilton* glass syringes are presented in Fig. 6(a). By exchanging the 100 μl syringe used in the presently studied apparatus for a 50 μl syringe, the number of steps required to produce a 1.1 mm diameter droplet increases from 116 to approximately 250. Thus, by significantly increasing the number of steps necessary to produce each droplet, one can achieve a narrower prediction interval.

B. Water droplet trajectories

The second goal for the water droplet generator is for successive droplets to follow the same trajectory to better predict the final landing point of a produced droplet. Figure 7(a) presents the $x - y$ position of each of the droplets generated to have diameters of (i) 1.10 mm, (ii) 1.79 mm, and (iii) 2.08 mm. The $x - y$ position of each droplet's centre of mass was measured for each of the separate experimental data sets, at increasing z. The spread shown in Fig. 7(b) is defined as the radius of the 95% confidence interval on the $x - y$ position of the droplet. The droplet generator was moved vertically in increments of 5 mm for the first 30 mm of descent from the generating tip in order to completely film the droplet phenomena that occur in this region. One additional dataset was collected for each droplet size at 102 mm vertical distance from the generating tip to elucidate the droplets' activity after considerable descent time. The 2.08 mm water droplets land within 0.7 mm of one another after a descent of 102 mm from the generating tip. The 1.79 mm water droplets land within

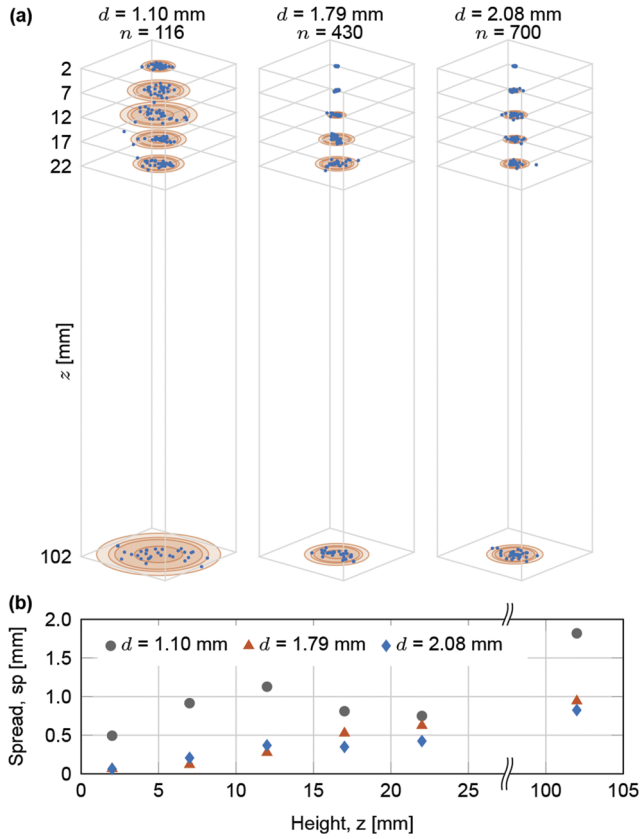

FIG. 7. (a) Measured $x-y$ position of the generated water droplets throughout their 100 mm descent. The rings shown where 50%, 90%, 95%, and 99% of the droplets were located at each height setting of the droplet generating apparatus, z. (b) Spread in the centre of masses of the droplets at each height setting of the droplet generating apparatus.

0.9 mm of one another after the 102 mm descent. In both of these cases, the spread in final landing site is well within the length of a single diameter of the droplet and is less than half of the diameter in the case of the 2.08 mm droplets. For the smallest droplet case, those having diameters of 1.10 mm, the final landing site of the droplets after 102 mm of descent is shown to be within 1.7 mm of one another or 1.5 droplet diameters.

The spread in the centre of mass of the droplets for each droplet size produced at each z-level is summarized in Fig. 7(b). The spreads of the location of the centre of masses of the larger droplets (those with diameters of 2.08 mm and 1.79 mm) are relatively small. Conversely, the smaller 1.10 mm droplets yield a larger spread in the location of their centre of masses. The force balance, as laid out in Eq. (1), shows that droplets are subjected to the same solid-liquid tension force, regardless of their diameter, when produced using the same tip (i.e., the solid-liquid contact area is constant with droplet volume). Therefore, smaller-massed droplets experience a higher net contribution of solid-liquid tension force over gravitational force than the larger-massed droplets. As such, any preferential solid-liquid attraction (i.e., localized hydrophilicity) that is occurring at the generating tip will have a larger effect on smaller-massed droplets. Local hydrophilic defects at the surface of the droplet generating tip necessitate either localized cohesive breakup of the droplet or de-wetting of the wet area for the droplet to be produced and descend. Rather than acting evenly throughout the circumference of the generating tip as in a hanging pendant, the localized adhesive force at the hydrophilic defects will result in a net positive lateral force on a detaching droplet. Therefore, any areas of the generating tip which are not superhydrophobic will result in a less well-defined trajectory, especially for droplets of lesser mass.

C. Water droplet volume oscillations

The final goal of the droplet generating apparatus is to produce water droplets which show minimal, reproducible oscillation in volume throughout their descent. This enables better predictability of the interaction between the generated droplet and any counter medium seen in applications. The oscillation in the volume of each water droplet produced is quantified in the present work as relative deformation, $\delta(z)$, according to Eq. (7). The assumed ellipsoidal shape of the water droplet as it oscillates throughout its descent is measured to determine the length of the major axis at vertical position z, $D_{major}(z)$. The length of the major axis is normalized to the diameter of a sphere with equivalent volume to the ellipsoid, $D_{eq}(z)$,

$$\delta(z) = \frac{D_{major}(z) - D_{eq}(z)}{D_{eq}(z)}. \tag{7}$$

The maximum relative deformation measured for each water droplet within each vertical section of high-speed filming is presented as boxplots in Fig. 8. As expected, the highest levels of relative deformation of the water droplets present themselves immediately upon generation from the droplet generating tip. To better elucidate the degree of solid-liquid interaction at the laser micromachined PTFE tip, still frames are presented in Fig. 9(a) which show the generation of representative water droplets. Of note is the elongation and retraction of the water droplet produced using 430 steps of the liquid syringe pump in Fig. 9(a–ii). The droplet elongates from the surface of the generating tip at 4.00 ms, retracts

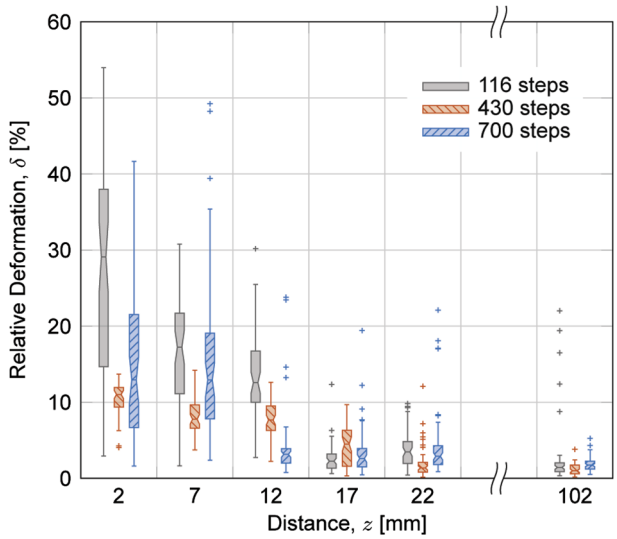

FIG. 8. Maximum spread in the centre of masses of the droplets produced using 116, 430, and 700 steps of the liquid syringe pump at each height setting of the droplet generating apparatus.

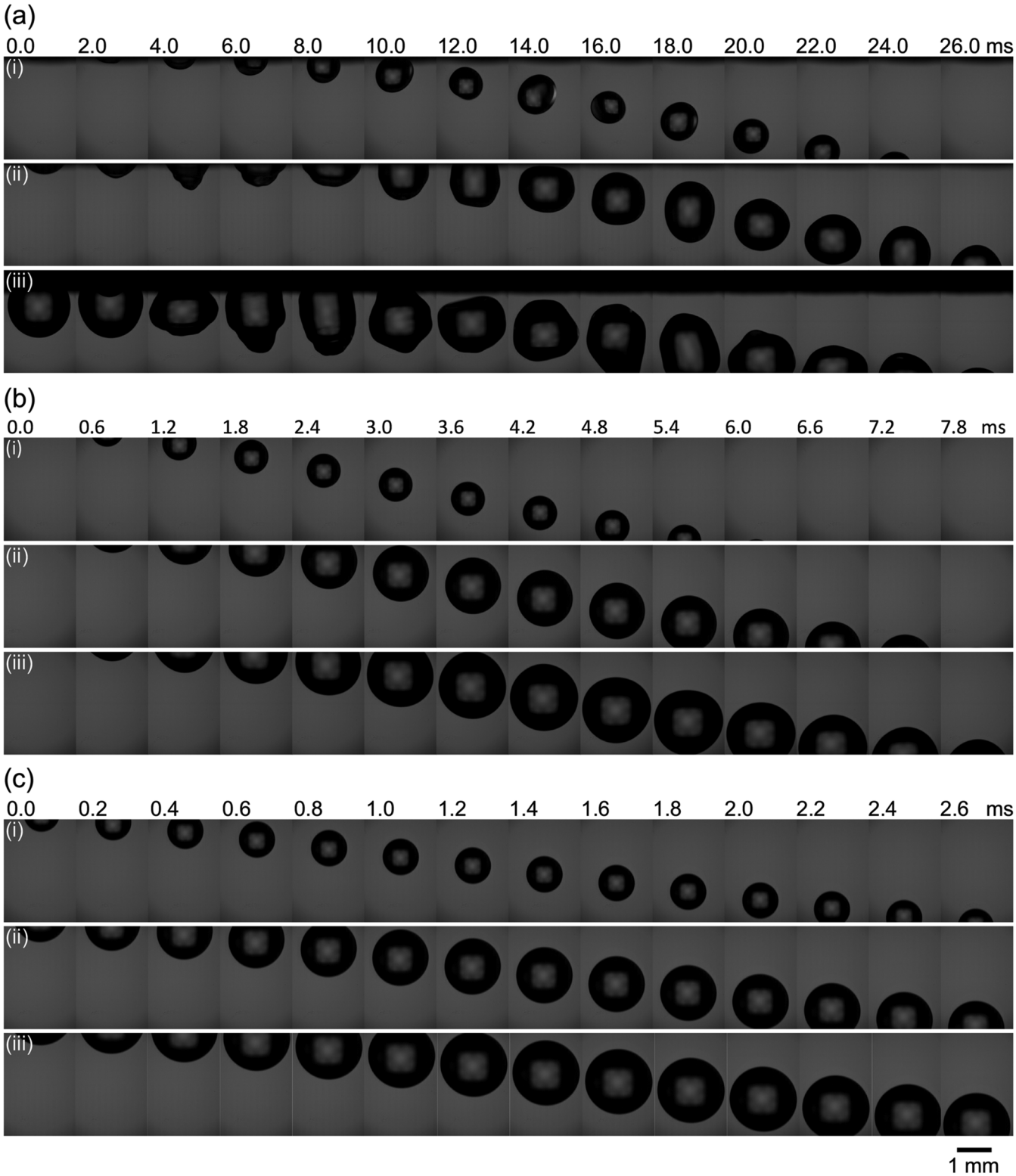

FIG. 9. Still frames of representative high-speed videos showing (a) the detachment of water droplets from the fs-laser micromachined PTFE tip. (b) Falling water droplets after 22 mm of descent from the PTFE generating tip and (c) falling water droplets after 102 mm of descent from the PTFE generating tip. Droplets were produced using (i) 116, (ii) 430, and (iii) 700 steps of the liquid syringe pump.

in the 6 ms that follow, and elongates once more at the 10.00 ms mark before fully detaching and forming an independent droplet that begins to descend. In the case of the generation of a larger water droplet, produced using 700 steps, presented in Fig. 9(a–iii), the elongation and retraction characteristics are even more pronounced. At 2 ms in the video, a dimple begins to appear within the droplet. The liquid that was inside the drilled hole of the PTFE generating tip has been pushed out by the pressure of the air being flowed through the tee-apparatus to eject the droplet. This suggests that the

solid-liquid interaction (i.e., wetting) occurring with the PTFE tip causes sufficiently strong attachment to allow the rim of the dimple to form. It is possible that a microstructure more susceptible to wetting is formed on the inner wall of the drilled hole when the patch is ablated over the end of the PTFE tip due to fluence reduction caused by laser pulses irradiating surfaces oriented non-perpendicularly to the beam path.[36] The parallel area of the drilled hole inner wall would receive a considerably reduced accumulated fluence than the perpendicular face of the PTFE tip. As discussed in the work of Liang *et al.*, the accumulated fluence of the patch ablated onto PTFE greatly affects the resulting microstructure.[32] Nonetheless, as sufficient air pressure is built up above the hanging 700 step liquid droplet, the dimple's rim detaches. The hanging droplet vibrates as discrete, minute detachments begin to occur. Full detachment of the wetted surface area begins to occur at 6 ms, causing the propagation of ripples on the surface of the droplet for the next 6 ms until full detachment at 12 ms in the presented video.

The oscillations in droplet volume decay with increasing distance from the generating apparatus. The general shape of the decay in oscillation is as to be expected, with the maximum relative deformations at each height, z, following the general damped oscillator exponential decay described in the early studies of Rayleigh and Lamb.[37–39] The oscillations decay to below 5% after 10 mm of descent from the generating tip. Figure 9(b) presents still frames of representative water droplets after having descended 20 mm from the generating tip. The level of oscillation in the volume exhibited by the majority of droplets after 10 mm of descent is sufficiently low that they have no bearing on the outcome of impact events with a solid surface. For context, studies on the impact of liquid droplets with a solid surface typically only include data from impact events where droplets had a relative deformation of less than 5% prior to collision to avoid false positives in splashing versus non-splashing.[7,11] The droplets in all three generated diameters decay to average relative deformations of around 2% after falling 102 mm from the droplet generating tip. Figure 9(c) presents still frames of representative water droplets of the three diameters produced after 102 mm of descent from the droplet generating tip.

IV. CONCLUSIONS

A droplet generating apparatus as an alternative to the methods currently employed has been designed and thoroughly tested to overcome the limitations in droplet size robustness, trajectory, and volume oscillation that are present with conventional drop generation methods. In separating the volume selecting step from the droplet generation step using a tee-apparatus, we have been able to produce droplets with highly accurate and precise volumes. The prediction interval for droplets made using 700 steps of the liquid syringe pumps was shown to be 5.3% of the droplet diameter. For droplets made using 430 steps of the liquid syringe pump, the prediction interval was shown to be 4.5% of the droplet diameter. The tee-apparatus is shown to possess no dead volume for the range of diameters tested by the close fit of the collected data to the operating curve established using the physical characteristics of the built generator. Further, a femtosecond laser micromachined superhydrophobic PTFE tip has enabled us to generate droplets over a range of diameters. The droplets generated using this novel apparatus possess oscillations in their volumes of less than 5% after 1 cm of descent from the generating tip. The superhydrophobic surface of the generating tip results in decreased solid-liquid interaction that proves beneficial in producing droplets which follow a similar trajectory to one another through successive generations. After 100 mm of descent, all droplets land within 1.5 diameters of one another. Our novel droplet generation system has successfully fulfilled the goals and hypotheses set out at the commencement of the work.

SUPPLEMENTARY MATERIAL

See supplementary material for a video overview of the droplet generation process, including representative high-speed videos of generated droplets.

ACKNOWLEDGMENTS

This work was supported financially by the Natural Science and Engineering Research Council of Canada (NSERC) through a Collaborative Research and Development (CRD) Grant with 3M Canada Company.

[1] R. H. Chen, *Liquid Crystal Displays: Fundamental Physics and Technology* (Wiley, Hoboken, NJ, 2011).
[2] R. D. Adams, *Adhesive Bonding: Science, Technology and Applications* (CRC Press, Boca Raton, FL, 2005).
[3] J. Varteresian, *Fabricating Printed Circuit Boards* (Newnes, New York, NY, 2002).
[4] H. H. Tønnesen and J. Karlsen, "Alginate in drug delivery systems," Drug Dev. Ind. Pharm. **28**, 621–630 (2002).
[5] D. Avnir, T. Coradin, O. Lev, and J. Livage, "Recent bio-applications of sol-gel materials," J. Mater. Chem. **16**, 1013–1030 (2006).
[6] A. Murua, A. Portero, G. Orive, R. M. Hernández, M. de Castro, and J. L. Pedraz, "Cell microencapsulation technology: Towards clinical application," J. Controlled Release **132**, 76–83 (2008).
[7] D. G. K. Aboud and A.-M. Kietzig, "Splashing threshold of oblique droplet impacts on surfaces of various wettability," Langmuir **31**, 10100–10111 (2015).
[8] C. D. Stow and M. G. Hadfield, "An experimental investigation of fluid flow resulting from the impact of a water drop with an unyielding dry surface," Proc. R. Soc. A **373**, 419–441 (1981).
[9] Z. Mohamed-Kassim and E. K. Longmire, "Drop impact on a liquid–liquid interface," Phys. Fluids **15**, 3263–3273 (2003).
[10] B. W. Faßmann, S. E. Bansmer, T. J. Möller, R. Radespiel, and M. Hartmann, "High velocity impingement of single droplets on a dry smooth surface," Exp. Fluids **54**, 1–18 (2013).
[11] S. S. Cacey, "Scaling of the splash threshold for low-viscosity fluids," Europhys. Lett. **106**, 24001–24006 (2014).
[12] K. Reil and J. Hallett, "An apparatus for the production of uniform sized water drops, at desired time intervals," Rev. Sci. Instrum. **40**, 533–534 (1969).
[13] X. Mao, L. Zhang, Z. Zhao, and F. Lin, "Generation of droplets via oscillations of a tapered capillary tube filled with low-viscosity liquids," Phys. Fluids **29**, 067104 (2017).
[14] A. U. Chen and O. A. Basaran, "A new method for significantly reducing drop radius without reducing nozzle radius in drop-on-demand drop production," Phys. Fluids **14**, L1–L4 (2002).
[15] S. Cheng and S. Chandra, "A pneumatic droplet-on-demand generator," Exp. Fluids **34**, 755–762 (2003).
[16] K.-C. Fan, J.-Y. Chen, C.-H. Wang, and W.-C. Pan, "Development of a drop-on-demand droplet generator for one-drop-fill technology," Sens. Actuators, A **147**, 649–655 (2008).

[17]B. Derby, "Inkjet printing of functional and structural materials: Fluid property requirements, feature stability, and resolution," Annu. Rev. Mater. Res. **40**, 395–414 (2010).
[18]A. A. Castrejón-Pita, J. R. Castrejón-Pita, and G. D. Martin, "A novel method to produce small droplets from large nozzles," Rev. Sci. Instrum. **83**, 115105 (2012).
[19]J. R. Castrejón-Pita, G. D. Martin, S. D. Hoath, and I. M. Hutchings, "A simple large-scale droplet generator for studies of inkjet printing," Rev. Sci. Instrum. **79**, 075108 (2008).
[20]A. Amirzadeh and S. Chandra, "Small droplet formation in a pneumatic drop-on-demand generator: Experiments and analysis," Exp. Therm. Fluid Sci. **34**, 1488–1497 (2010).
[21]C. Tropea, A. L. Yarin, and J. F. Foss, *Springer Handbook of Experimental Fluid Mechanics* (Springer E-Books, Berlin, 2007).
[22]T. Tate, "On the magnitude of a drop of liquid formed under different circumstances," Philos. Mag. **27**, 176–180 (1864).
[23]G.M. O'Shea and A. M. Sun, "Encapsulation of rat islets of Langerhans prolongs xenograft survival in diabetic mice," Diabetes **35**, 943–946 (1986).
[24]A. Kikuchi, M. Kawabuchi, M. Sugihara, Y. Sakurai, and T. Okano, "Pulsed dextran release from calcium-alginate gel beads," J. Controlled Release **47**, 21–29 (1997).
[25]T. Maitra, C. Antonini, M. K. Tiwari, A. Mularczyk, Z. Imeri, P. Schoch, and D. Poulikakos, "Supercooled water drops impacting superhydrophobic textures," Langmuir **30**, 10855–10861 (2014).
[26]Y. H. Yeong, J. Burton, E. Loth, and I. S. Bayer, "Drop impact and rebound dynamics on an inclined superhydrophobic surface," Langmuir **30**, 12027–12038 (2014).
[27]E. R. Lee, *Microdrop Generation* (CRC Press, Boca Raton, FL, 2003).
[28]P. C. Duineveld, M. M. de Kok, M. Buechel, A. Sempel, K. A. H. Mutsaers, P. van deWeijer, I. G. J. Camps, T. van deBiggelaar, J.-E. J. M. Rubingh, and E. I. Haskal, "Ink-jet printing of polymer light-emitting devices," in *International Symposium on Optical Science and Technology* (SPIE, 2002), Vol. 4464, p. 9.
[29]N. Reis and B. Derby, "Ink jet deposition of ceramic suspensions: Modeling and experiments of droplet formation," MRS Proc. **625**, 117 (2011).
[30]S. Kosch and N. Ashgriz, "Note: A simple vibrating orifice monodisperse droplet generator using a hard drive actuator arm," Rev. Sci. Instrum. **86**, 046101 (2015).
[31]A. Vinokhodov, M. Krivokorytov, Y. Sidelnikov, V. Krivtsun, V. Medvedev, V. Bushuev, K. Koshelev, D. Glushkov, and S. Ellwi, "Stable droplet generator for a high brightness laser produced plasma extreme ultraviolet source," Rev. Sci. Instrum. **87**, 103304 (2016).
[32]F. Liang, J. Lehr, L. Danielczak, R. Leask, and A.-M. Kietzig, "Robust non-wetting PTFE surfaces by femtosecond laser machining," Int. J. Mol. Sci. **15**, 13681–13696 (2014).
[33]R. H. Dettre and R. E. Johnson, "Contact angle hysteresis," in *Contact Angle, Wettability, and Adhesion*, Advances in Chemistry Vol. 43 (American Chemical Society, 1964), Book section 8, pp. 136–144.
[34]B. Wijnen, E. J. Hunt, G. C. Anzalone, and J. M. Pearce, "Open-source syringe pump library," PLoS One **9**, e107216 (2014).
[35]N. Otsu, "A threshold selection method from gray-level histograms," IEEE Trans. Syst., Man, Cybern. **9**, 62–66 (1979).
[36]E. J. Y. Ling, J. Saïd, N. Brodusch, R. Gauvin, P. Servio, and A.-M. Kietzig, "Investigating and understanding the effects of multiple femtosecond laser scans on the surface topography of stainless steel 304 and titanium," Appl. Surf. Sci. **353**, 512–521 (2015).
[37]Lord Rayleigh, "On the capillary phenomena of jets," Proc. R. Soc. A **29**, 71–97 (1879).
[38]H. Lamb, "On the oscillations of a viscous spheroid," Proc. London Math. Soc. **s1-13**, 51–70 (1881).
[39]H. Lamb, *Hydrodynamics* (Cambridge University Press, Cambridge, 1932).